# A microfluidic optical platform for real-time monitoring of pH and oxygen in microfluidic bioreactors and organ-on-chip devices

Seyed Ali Mousavi Shaegh,[1,2] Fabio De Ferrari,[1,2,3] Yu Shrike Zhang,[1,2,4] Mahboubeh Nabavinia,[1,2,5] Niema Binth Mohammad,[1,2,6] John Ryan,[1,2,7] Adel Pourmand,[1,2,8] Eleanor Laukaitis,[1,2,9] Ramin Banan Sadeghian,[1,2,10] Akhtar Nadhman,[1,2,11] Su Ryon Shin,[1,2] Amir Sanati Nezhad,[1,2,12] Ali Khademhosseini,[1,2,4,10,13,14] and Mehmet Remzi Dokmeci[1,2,4,a)]

[1]*Biomaterials Innovation Research Center, Department of Medicine, Brigham and Women's Hospital, Harvard Medical School, Boston, Massachusetts 02139, USA*
[2]*Harvard-MIT Division of Health Sciences and Technology, Massachusetts Institute of Technology, Cambridge, Massachusetts 02139, USA*
[3]*Department of Electronics and Telecommunications, Politecnico di Torino, 10129 Torino, Italy*
[4]*Wyss Institute for Biologically Inspired Engineering, Harvard University, Boston, Massachusetts 02139, USA*
[5]*Department of Chemical Engineering, Sahand University of Technology, 5331711111 Tabriz, Iran*
[6]*Faculty of Applied Science and Engineering, University of Toronto, Toronto, Ontario M5S 3E3, Canada*
[7]*Department of Physics, Massachusetts Institute of Technology, Cambridge, Massachusetts 02139, USA*
[8]*Department of Electrical Engineering, Sahand University of Technology, 5331711111 Tabriz, Iran*
[9]*Department of Biological Engineering, Massachusetts Institute of Technology, Cambridge, Massachusetts 02139, USA*
[10]*WPI-Advanced Institute for Materials Research, Tohoku University, Sendai 980-8577, Japan*
[11]*Sulaiman Aba Al Khail Centre for Interdisciplinary Research in Basic Sciences (SA-CIRBS), International Islamic University, Islamabad, Pakistan*
[12]*BioMEMS and Bioinspired Microfluidic Laboratory, Department of Mechanical and Manufacturing Engineering, University of Calgary, Calgary, Alberta T2N 1N4, Canada*
[13]*Department of Physics, King Abdulaziz University, Jeddah 21569, Saudi Arabia*
[14]*College of Animal Bioscience and Technology, Department of Bioindustrial Technologies, Konkuk University, Hwayang-dong, Kwangjin-gu, Seoul 143-701, South Korea*

(Received 12 February 2016; accepted 17 June 2016; published online 26 August 2016)

There is a growing interest to develop microfluidic bioreactors and organ-on-chip platforms with integrated sensors to monitor their physicochemical properties and to maintain a well-controlled microenvironment for cultured organoids. Conventional sensing devices cannot be easily integrated with microfluidic organ-on-chip systems with low-volume bioreactors for continual monitoring. This paper reports on the development of a multi-analyte optical sensing module for dynamic measurements of pH and dissolved oxygen levels in the culture medium. The sensing system was constructed using low-cost electro-optics including light-emitting diodes and silicon photodiodes. The sensing module includes an optically transparent window for measuring light intensity, and the module could be connected directly to a perfusion bioreactor without any specific modifications to the microfluidic device design. A compact, user-friendly, and low-cost electronic interface was developed to control the optical transducer and signal acquisition from photodiodes. The platform enabled convenient integration of the optical sensing module with a microfluidic bioreactor. Human dermal fibroblasts were cultivated in the bioreactor, and the

a)Author to whom correspondence should be addressed. Electronic mail: mdokmeci@rics.bwh.harvard.edu

values of pH and dissolved oxygen levels in the flowing culture medium were measured continuously for up to 3 days. Our integrated microfluidic system provides a new analytical platform with ease of fabrication and operation, which can be adapted for applications in various microfluidic cell culture and organ-on-chip devices. *Published by AIP Publishing*. [http://dx.doi.org/10.1063/1.4955155]

## I. INTRODUCTION

Microengineered cell culture models built inside microfluidic bioreactors and organ-on-chip devices are enabling biomimetic microsystems that provide key working units of living human organs.[1] These cell culture models are primarily designed to provide more trustworthy predictions of drug effectiveness and safety in humans in comparison with the existing preclinical methods.[2] A physiologically relevant microengineered cell culture model should replicate the three-dimensional (3D) microarchitecture of intact organs with realistic tissue-tissue interfaces and organ-specific physical and biochemical microenvironment.[2,3] Such biomimetic microsystems allow for short-term and long-term analysis of organ-specific responses to microenvironmental stimuli including induced physical forces, drugs, and toxins.[1,4–8]

Microfluidic bioreactors and organs-on-chip microsystems are generally perfused by a common culture medium as a blood surrogate.[9] Any changes in the physicochemical properties of the blood surrogate may cause undesirable changes in the physiology of the organoids and result in deteriorating the prediction accuracy of the organ-on-chip models for drug screening studies. For instance, extracellular acidity ($pH_e$) affects different biological processes[10] such as immune function,[11] matrix synthesis by chondrocytes,[12] and contractile function of cardiac muscles.[13] In addition, $pH_e$ may be altered by the organoids. For example, it can become acidic[14] in certain environments such as inside tumors with $pH_e$ values in the range of 6.2–6.9.[15,16] Oxygen tension also plays a critical role in cellular activities.[17] Insufficient oxygen delivery to cells may cause variations in cellular metabolism,[18] physiological pathways,[19] and tissue remodeling,[20] while high oxygen concentrations may lead to increased generation of reactive oxygen species in pathological levels with possible damage to cellular components.[21]

Thus, it is important to monitor the physicochemical parameters within the culture medium.[22–24] In addition, proper control of the oxygen tension is a critical task for multi-organ-on-chip microsystems,[9,25,26] where each organ construct may need a unique microenvironment with special levels of dissolved oxygen.[17] Hence, the development of microfluidic platforms with integrated multi-analyte sensing capabilities for in-line monitoring of physicochemical parameters of organ constructs is needed to fully enable the use of organs-on-chip microsystems for *in vitro* analysis of cellular functions.[27,28]

Given the limited volume of microscale bioreactors, the sensing system should be miniature in size and should possess minimal chamber volume and be easily integratable with a microfluidic organ-on-chip platform. To facilitate the operation and adaptability of such integrated systems, a sensing device should ideally be equipped with electronic control and automated inference for data acquisition, visualization, and storage.[25] Microfluidic detection methods are highly suited for integration with organ-on-chip devices due to their potential for the analysis of low-volume liquids and high degree of automation.[29] A variety of microfluidic optical and electrochemical techniques have been developed to measure oxygen[22,30–38] and pH[31,34,37,39–44] for cell-based studies. Moreover, in some instances, the optical methods are preferred over electrical methods since they do not require electrical connections and electrodes which may be prone to biofouling and corrosion. In addition, they are also less vulnerable to electrical/electrochemical interferences introduced by the biochemical species present in the cell culture solution.[25] The optical measurement of pH and oxygen mainly relies on the detection of alterations in the optical property of oxygen and pH indicators. Light absorption or fluorescent intensity of an indicator is monitored when the oxygen or pH of the environment is altered.[45] Optical probes could be less prone to drifts or interferences caused by the ions, drugs, or proteins present in the cell culture medium. Also, in general, the performance of optical sensors is not influenced by the flow rates. Thus, an

optical sensor can perform consistent and reliable measurements where a dynamic range of flow rates for the perfusion of culture medium is required.

Here, we introduce an optical multi-analyte sensing module integrated with a microfluidic bioreactor for in-line monitoring of pH and dissolved oxygen in the circulating culture medium. The sensing module comprises of a microfluidic detection chamber integrated with low-cost solid-state optical components (Si photodiodes and light emitting diode, LED). This approach enabled the fabrication of a compact and miniature detection system for pH and oxygen measurements, which was an advantage over the bulky spectrophotometry[46] or microscopy techniques.[47,48] To measure pH levels, direct measurement of optical absorption by flowing culture medium containing phenol red was conducted with fixed electro-optics installed above and below the detection chamber. A broadband LED was used as an excitation source, while a Si photodiode was employed to detect the amount of light absorbed while passing through the media. Measurement of oxygen levels was performed using an oxygen-sensitive dye immobilized within a film inside the detection chip. A high-power blue LED was used to excite the dye, while two Si photodiodes were used to measure the degree of quenching in the luminescent intensity. The sensing module was then integrated with a microfluidic bioreactor containing human dermal fibroblasts (HDFs) to construct a microfluidic platform for continuous monitoring of pH and oxygen levels in the perfused culture medium. In order to achieve accurate monitoring, an electronic circuit was developed to conduct required signal filtering and amplification for the pH and oxygen sensors. In addition, a compact and self-contained electronic interface was realized using a custom-designed Arduino™-based microcontroller integrated with a touch screen liquid crystal display (LCD). The microcontroller was designed to control the operation of the sensors including data acquisition and real-time data display. The touch screen LCD enabled the user to record and visualize data in real-time, providing direct control over the operation of the sensor.

## II. MATERIALS AND METHODS

### A. System concepts and the design of the multi-analyte sensing module

The aim of this study was to develop a compact multi-analyte optical sensing module for easy integration with a bioreactor in a perfusion microfluidic platform. The sensing module should have a transparent window, and the module should have fluidic connections to the perfusion system with cells inside. The sensors were constructed on a single chip to enable connection of the sensing module to the bioreactor (Figs. 1(a) and 1(b)). The whole fluidic chip was made from laser-machined poly(methyl methacrylate) (PMMA) layers bonded together using double-sided adhesives. The length and width of the fluidic channel were 50 mm and 3 mm, respectively. The height of the channel was characterized within a range from 0.25 mm to 1 mm. Then, further calibration experiments were carried out in a channel with the height of 0.5 mm. The electronic circuitry was positioned and mounted firmly under the detection channel using screws. Plastic tubing (Cole-Parmer) with a fast-drying epoxy (Devcon 5 Minute 14250 Epoxy Resin) was used to make fluidic connections wherever needed. Cells adhered and then proliferated in the bioreactor while they were exposed to the perfusion cell culture medium (Figs. 1(c) and 1(d)). The pH and oxygen levels in the culture medium were monitored while the medium moved through the sensing module. The system fluidics was pressure-driven using a peristaltic pump (Cole-Palmer, 4-channel, 74906-03) (Fig. 1(e)).

### B. Fabrication of the pH sensor

Prior to fabrication of the multi-analyte sensing module, individual pH and oxygen sensors were fabricated and characterized. The operation of the pH sensor was based on the detection of the level of light absorbed by phenol red in the culture medium. Phenol red is a water-soluble molecule that is often used to determine the pH levels in cell culture experiments. The amount of light absorbed through a phenol red-containing solution is a function of pH, and its color is known to change from yellow to red over physiological pH ranges (Figs. 2(a) and 2(b)). To characterize the amount of light absorbed in a phenol red solution having different

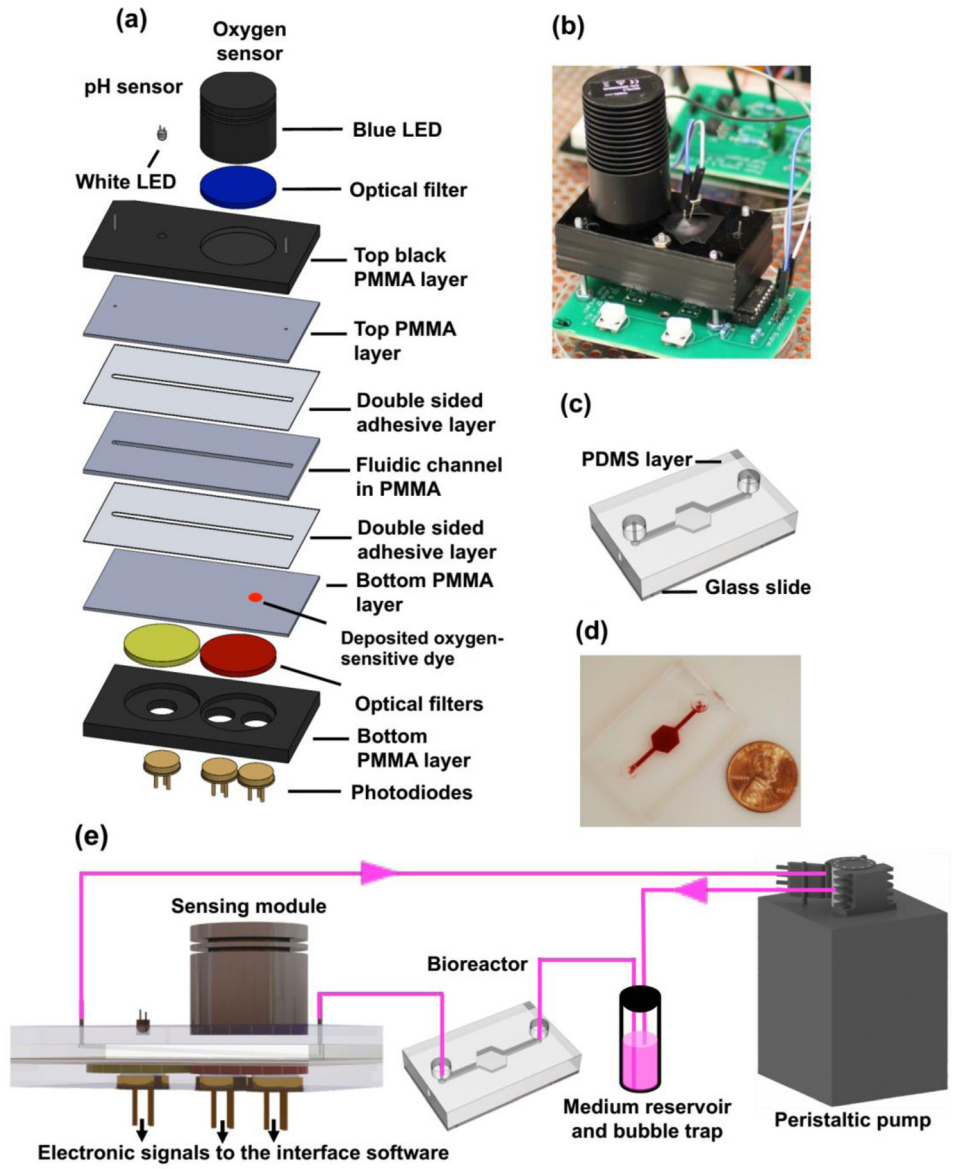


FIG. 1. Fabricated devices and test setup. (a) Exploded view of the sensing module for pH and oxygen measurement, (b) photograph of the fabricated sensing module, (c) schematic of the bioreactor, (d) photograph of the fabricated bioreactor, (e) schematic of the sensing module integrated with peristaltic pump, culture medium reservoir, and bioreactor in a fluidic system.

pH values, solutions of Dulbecco's Modified Eagle Medium (DMEM, Life Technologies) in pH of 6, 7, and 8 were tested using a microvolume UV-visible spectrophotometer (ND-1000, Nano-Drop). The peak absorption occurred at 560 nm. We also noticed that as the pH value of the solution was increased, the light absorbed through culture medium also increased. To characterize the amount of light absorbed by the phenol red solution with different pH values, a low-cost optical monitoring system was developed. An unpackaged white LED (LEDWE-15, Thorlabs) was used as the illumination source. A Si photodiode (FDS100, Thorlabs), filtered by a long-pass optical filter (FGL515, 515 nm, Thorlabs), was employed as the detector to quantify the amount of absorbed light from the LED-emitted light travelling through the fluidic channel (Figs. 2(c) and 2(d)). The distance of the light path was determined by the height of the fluidic channel, which affected the detection sensitivity. In the optical system, the LED light source was placed above the microfluidic detection chamber, and the photodiode was placed below the chamber to detect the amount of light absorbed by the medium (Fig. 2(e)). The detection

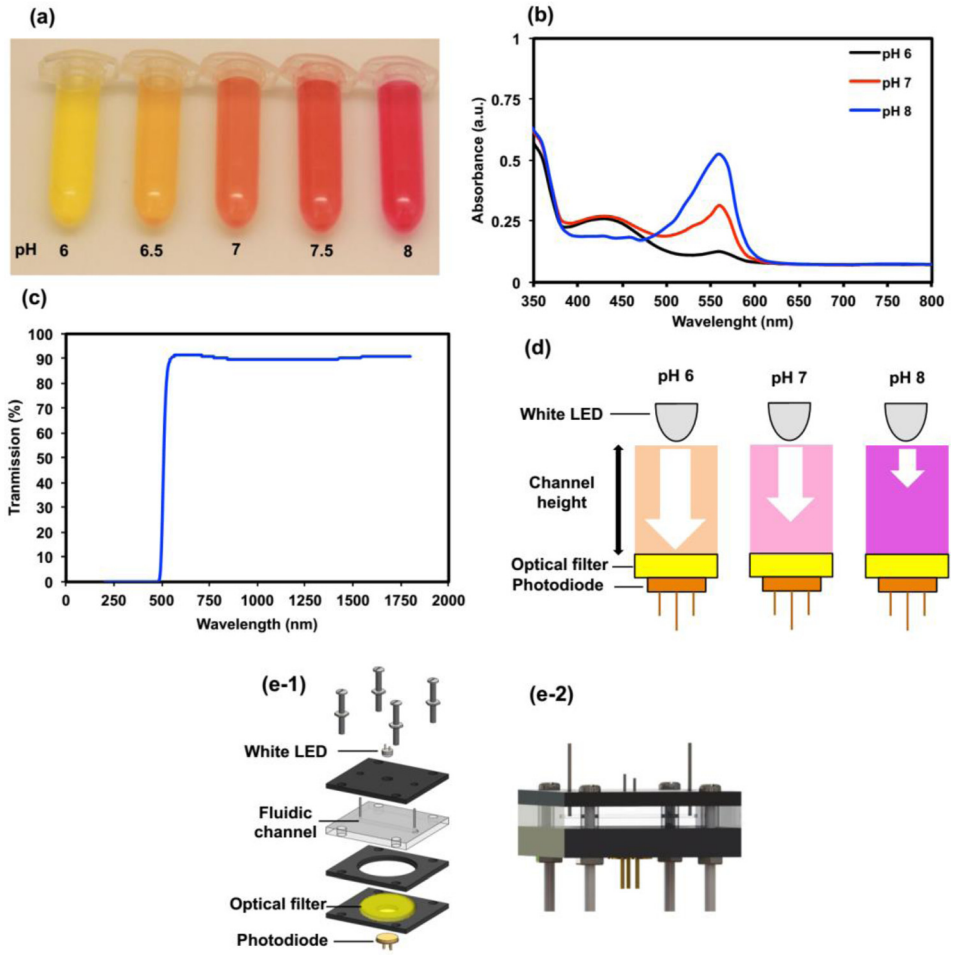


FIG. 2. Working principle of pH sensing in cell culture medium and sensor characterization data. (a) Color change of phenol red containing culture medium (DMEM) at different pH values, (b) absorbance spectra of culture medium at pH values of 6, 7, and 8, (c) transmission spectra of the employed optical filter, (d) schematic of detecting level of light absorption in culture medium using solid-state optics, (e) schematic of the fabricated fluidic detection chamber with integrated optical components: (e-1) exploded view and (e-2) assembled view.

chamber was generated from the laser-machined PMMA slabs bonded together employing pharmaceutical grade pressure-sensitive adhesive tape (ARcare® 90445, Adhesive Research, USA). ARcare 90445 is a clear, thin, and flexible polyester substrate coated on both sides with a medical grade pressure-sensitive adhesive. The double-sided tape is protected by a clear polyester release liner on both sides. The dimensions of the tape are 1 mil thick substrate; 1.1 mils thick adhesive (both sides); thickness (without liners): 3.2 mils; and the total thickness (including liners): 7.2 mils. In short, the adhesive has a thickness of 28 $\mu$m (1.1 mils), and the total thickness of the tape, including the plastic film coated with adhesive on both sides, without liners is 81 $\mu$m (3.2 mils). Thus, for the overall height of the channel, the thickness of the pressure-sensitive tape should be added to the thickness of the PMMA slab used for the fabrication of the channel (e.g., $0.25\,\text{mm} + 2 \times 0.081\,\text{mm}$).

The whole detection chamber was sandwiched between two black PMMA laser cut pieces to reduce the interference caused by light from the environment.

To characterize the pH sensor, DMEM with different pH levels were prepared by the titration of diluted HCl and NaOH solutions to the medium. pH of the prepared solutions was measured using a commercial benchtop pH meter (Fisher Science Education) calibrated at pH values of 4, 7, and 10. The response of the pH sensor was characterized for the pH range of 6–8 (6,

6.5, 7, 7.5, 8), as it provided a physiological range for cell culture applications. The solutions with different pH values were used immediately after preparation. 1 ml of each solution was used for each characterization experiment, assuring that the entire detection channel was filled with the solution and any excess solution remaining from the previous test was removed from the channel. The characterization experiments were conducted using reference solutions with different pH levels, and trials were run for ascending and descending pH values.

### C. Fabrication of oxygen sensor

The operation of the oxygen sensor relies on the quenching of the luminescent intensity of a fluorophore in the presence of oxygen (Fig. 3(a)). Optical oxygen sensors generally employ an oxygen-quenchable luminescent dye, which has a fast response and has linear output. Moreover, they are not susceptible to drift caused by consumption of oxygen by the sensing dye.[32,49,50] In this study, an oxygen-sensitive fluorophore, $[Ru(dpp)_3]^{2+}Cl_2$–tris(4,7-diphenyl-1,10-phenanthroline)ruthenium(II) chloride (Sigma-Aldrich), was used as the oxygen indicator, due to its high photostability and moderate brightness.[33] It has a maximum excitation at a wavelength of 463 nm, while the maximum emission occurs at 618 nm.[33] Similar to the pH sensor, a detection chamber was fabricated which housed an oxygen-sensitive dye deposited at the bottom of the chamber. To fabricate the sensor, the luminophore powder was dissolved in ethanol in 1 mg/ml concentration. A droplet of the solution (2 $\mu$l) was dispersed on the substrate using shadow masking technique. The substrate was placed in dark for solvent evaporation. In order to use the dye for dissolved oxygen measurements in an aqueous environment, a thin layer of polydimethylsiloxane (PDMS) (10:1, base monomer: curing agent) was spin-coated over the deposited dye at a spin rate of 500 rpm for 30 s and a subsequent spin at 6000 rpm for 1 min. The PDMS layer protects the dye from direct contact with the culture media while it allows for oxygen diffusion to the oxygen sensing area. The dye was then incorporated within the detection chamber using the fabrication process explained for the pH sensor. To excite the deposited dye, a high-power blue LED (M470L3, 470 nm, 650 mW, Thorlabs) was positioned directly above the fluidic detection channel (Figs. 3(b) and 3(c)). The blue illumination was filtered using a band-pass excitation filter (FGB7, 435–500 nm, Thorlabs) before entering the detection chamber. Two Si photodiodes (FDS100, Thorlabs), in antiparallel configuration, were placed below the detection channel, shielded and filtered by a long-pass filter (FGL610, 610 nm, Thorlabs) mounted above the photodiodes. Both photodiodes were viewing the light through the fluidic channel, but only one photodiode could view the light emitted from the dye. This configuration allowed for a differential readout between the luminescent intensity emitted from the dye and the background light intensity arising mainly from the illumination caused by the blue LED.

Characterization of the oxygen sensor was carried out both for gaseous and dissolved oxygen. Dynamic response of the sensor was initially conducted using gaseous nitrogen and air,

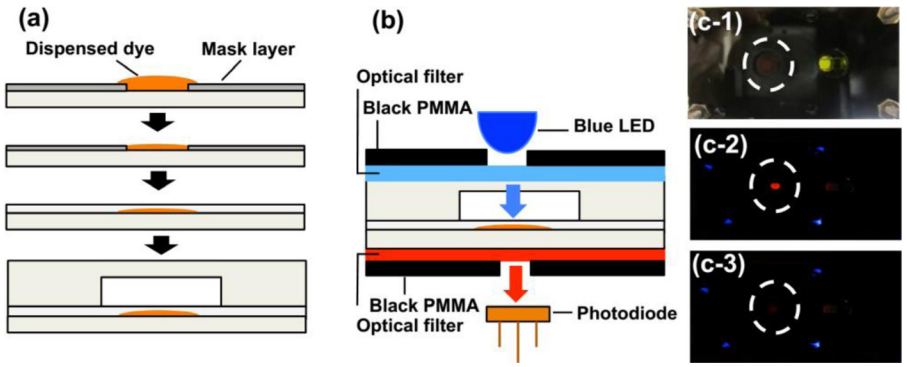


FIG. 3. Working principle of oxygen sensing. (a) Deposition process of the oxygen-sensitive dye, (b) arrangement of deposited dye in the detection chamber for signal read out, (c) response of the sensor to gaseous oxygen with different concentrations: (c-1) Blue excitation LED was off, (c-2) Blue LED was ON with $N_2$ gas flow, (c-3) Blue LED was ON with air flow (21% oxygen).

and a mixture of air and nitrogen with 12% oxygen content. To make the gas mixture, nitrogen and air were mixed in a custom-made chamber. A commercial oxygen probe (OceanOptics, Florida, USA) was used to measure the oxygen content in the mixture before it was introduced into the sensor. Dynamic response of the sensor to dissolved oxygen in aqueous solutions was characterized using reference solutions. Reservoirs of culture medium were bubbled with nitrogen (0% $O_2$) and air (21% $O_2$) for a minimum time of 1 h. Calibration tests of the luminescent intensity were carried out through perfusing the sensor with pure nitrogenated and oxygenated solutions and a 1:1 (aerated: nitrogenated) mixture solution. The prepared solutions were immediately injected into the oxygen sensor using a syringe.

### D. Hardware for signal readout

An analog circuit was designed and fabricated to convert the photocurrent, generated by the photodiodes of pH and oxygen sensors, into electrical potential (see Figs. S1a and S1b in the supplementary material).[51] The circuit for each sensor consisted of a transimpedance amplifier to convert the photocurrent into a voltage, and an operational amplifier with a positive gain feedback configuration. One photodiode was employed for pH sensing, while the oxygen sensor consisted of two photodiodes connected in antiparallel configuration. For each sensor, an amplifier (MCP604, Microchip) was adapted to convert the photocurrent into a voltage. A 1 MΩ resistor in parallel with a capacitor was adapted in the feedback loop of the transimpedance amplifier to filter low and high frequency noise. The output of the first stage was connected to the positive input of the second amplifier. The maximum output voltage of the circuit was 5 V, which was determined by the second-stage amplifier. Since the measured signal was assumed to be constant during each measurement, a cut-off frequency in the order of few hertz was chosen.

In order to generate a stable voltage to power broadband LED and perform measurements, a power supply circuit was designed and implemented using an adjustable positive-voltage regulator (LM317, Texas Instruments) (see Figs. S1c and S1d in the supplementary material).[51] The frequency for white LED illumination was regulated with LabVIEW or Arduino microcontroller through an optocoupler (4N35, Texas Instruments). Due to the high power requirement of the blue LED, a solid-state relay was adapted to interface it with the LabVIEW program.

### E. Electronic interface for control of transducers and signal acquisition

Initially, a software controller was developed in LabVIEW to regulate the operation of the LEDs, record signals generated by the photodiodes, and perform processing of the recorded data to produce averaged data points. To enhance portability and integration of the sensing system, a stand-alone electronic interface was implemented in Arduino microcontroller (Mega 2560, SmartProjects, Italy) (see Fig. S2 in the supplementary material).[51] Arduino board with its associated integrated software environment provides a cost-effective yet powerful open-source platform to implement hardware control of transducers and signal acquisition from detectors,[52,53] and it has been already implemented for some microfluidic devices.[54,55] In this project, the Arduino microcontroller was integrated with a touch screen LCD (SainSmart 3.2″ TFT LCD Display + Touch Panel + PCB Adapter SD Slot for Arduino 2560 UNO R3 Mega Nano Robot) to provide an interactive graphical user interface (GUI) and a secure digital (SD) card. GUI enabled a user to start/stop data acquisition and visualize data points on the LCD. The microcontroller communicated with the SD card to read the frequency of data acquisition and to store real-time measurements. In this way, the control system provided a compact and user-friendly interface and control system in which its operation is independent from a computer.

### F. Fabrication of bioreactor

The bioreactor consisted of a fluidic chamber fabricated in PDMS, which was capped with a glass slide using plasma treatment (Figs. 1(c) and 1(d)). The fabricated bioreactor was stored in air for few days before use to achieve high oxygen diffusion through PDMS.[38] Owing to the

fact that PDMS is highly gas permeable,[56] the PDMS chamber enabled the diffusion of oxygen and $CO_2$ to the flowing culture medium.[57] Fluidic chamber was fabricated by casting PDMS onto a laser cut PMMA mold in a hexagonal shape. PDMS slab was peeled off from the mold after it was cured at 80 °C for 1 h. A glass slide was bonded to the PDMS after plasma treatment process for 90 s. The bioreactor was placed in series with the fluidic system via plastic tubing. The fluidic system consisted of a peristaltic pump, a reservoir that contained cell culture medium, a bioreactor, and the sensing module for pH and oxygen measurements, (Fig. 1(e)). The chamber area of the bioreactor was 53 $mm^2$ with a depth of 2 mm. The volume of the bioreactor was approximately 106 $\mu$l. The volume of the culture medium in the reservoir was 1.5 ml. The flow rate of the culture medium was 200 $\mu$l/h. Also, the volumes of the sensing module and the tubing were approximately 12.3 $\mu$l and 21 $\mu$l, respectively. The total length of the tubing was 30 cm.

In order to investigate gas permeability of the bioreactor, an oxygen sensor was fabricated with a fluidic chamber made of PDMS. To study the gas permeability of the chamber, first, the chamber of the sensor was continuously perfused with a nitrogen-bubbled solution (0% oxygen), and $O_2$ levels were measured. Then, perfusion was stopped which allowed for the diffusion of the environmental oxygen into the chamber containing the oxygen-sensitive dye. During this process, $O_2$ levels were measured using the oxygen sensor.

### G. Cell culture in bioreactor

HDFs (BJ, CRL 2522, ATCC, Manassas, VA) were used for cell culture in the bioreactor. They were initially grown in cell culture flask. Prior to seeding the cells into the bioreactor, the whole set-up was sterilized by UV and a perfusion of penicillin-streptomycin (300×) solution. DMEM added with 10% fetal bovine serum (Gibco) and antibiotics, 100 U $ml^{-1}$ penicillin (Sigma-Aldrich), and 100 U $ml^{-1}$ streptomycin (Gibco) was used for both culturing process and perfusion in the bioreactor at 37 °C.

HDFs were harvested from sub-confluent cultures, detached using 0.1% trypsin with 1 mM EDTA (Sigma-Aldrich) in phosphate-buffered saline (PBS) and re-suspended in DMEM medium containing 10% fetal bovine serum (FBS) and 100× Pen-Strep to prepare a concentration of $2 \times 10^6$ cells $ml^{-1}$. The cells were injected into the bioreactor using a 1-ml syringe to produce an initial cell density of $4 \times 10^5$ cell $cm^{-2}$. Subsequently, after cell seeding, inlet and outlet of the bioreactor were blocked using two metal bars (Instech, 20GA SS Coupler, 15 mm long), and the system was placed in an incubator for 24 h to create a confluent layer of cells adhered to the glass slide in the bioreactor. Then, the bioreactor was placed in the fluidic system to monitor pH and oxygen levels. Cell viability and proliferation were measured by live-dead fluorescence assay. For control cultures, cells were seeded in standard tissue culture (TC) 6-well plates as well as bioreactors with static conditions at a density of $3 \times 10^5$ cells $ml^{-1}$.

## III. RESULTS AND DISCUSSION

### A. Characterization of the pH sensor

There are a few design parameters that can affect the sensitivity of the pH measurements including (i) the concentration of the dissolved phenol red in culture medium, (ii) intensity of illumination from the broadband LED, and (iii) the height of the detection chamber. To simplify the optimization of the sensor design, regular DMEM, which contains 15 mg/l of phenol red, was used. Also, the voltage source for the broadband LED, provided by the power supply circuit, was fixed at 3 V. The effect of channel height on the light absorbance of phenol-red containing culture medium was investigated for channel heights of 0.25 mm, 0.5 mm, and 1 mm (Fig. 4(a)). For each channel height, experiments were conducted at pH values of 6, 6.5, 7, 7.5, and 8. Each experiment was repeated three times. Experiments were conducted using solutions with different pH values, and trials were run for ascending and descending pH values. The output voltages, generated by the photodiode, were measured and then normalized with respect to the potential associated with pH 6 ($V/V_{pH\ 6}$). As the channel height increased, the sensitivity of

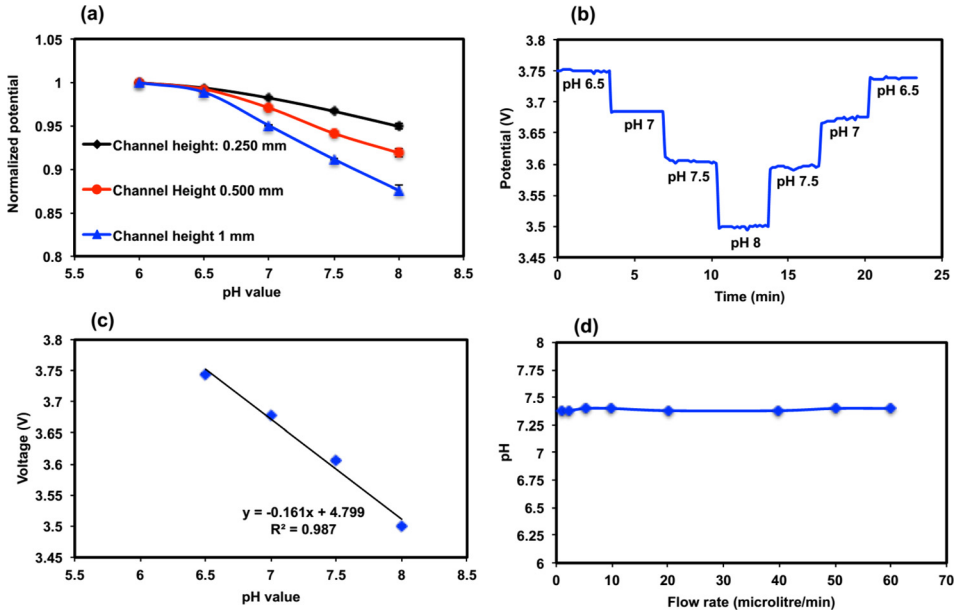


FIG. 4. Characterization curves of the pH sensor. (a) Effect of the channel height on the level of absorption detected by the photodiode, (b) step experiment to show the sensitivity of the pH sensor built in a channel with a height of 0.5 mm, (c) calibration curve of the pH sensor with a channel height of 0.5 mm, (d) effect of flow rate on the sensitivity of the pH sensor; tests done using a solution with a pH of 7.4. Error bars for different points of (c) and (d) are less than ±0.002 and not visible on figures.

the sensor to pH changes improved (Fig. 4(a)). This was mainly due to the fact that the path length of light travelling through the channel increased as the channel height increased, which resulted in enhanced absorption. Hence, the sensitivity of the pH sensor and the total volume of the detection chamber can be tailored by changing the height of the channel. In addition, for each channel height, the variations in the output voltage of the sensors were minimal for pH values from 6 to 6.5, whereas larger values in signal response were observed for pH values from 6.5 to 8. The sensor showed a linear response for pH values from 6.5 to 8. This behavior of the sensor was in agreement with the response of a phenol red-based pH sensor characterized with a spectrophotometer.[46] Therefore, the pH sensor was further characterized and optimized for the pH range of 6.5–8. Also, signal-to-noise ratio (SNR) for the pH sensor was 39.2 dB calculated using a wavelet-based signal-denoising algorithm.[58] The Ardruino module was able to detect variations of 5 mV. This accuracy allowed for detecting pH variations as small as 0.03 pH. The bandwidth was fixed to 0.34 Hz by the analog low-pass filter of the circuit.

In order to provide a compromise between high sensitivity of the pH sensor and the total volume of the detection chamber, channel height of 0.5 mm was selected for the fabrication of the pH sensor. Fig. 4(b) shows the response of the sensor with a channel height of 0.5 mm to dynamic pH changes from 6.5 to 8. Solutions at varying pH values were perfused into the sensor at a flow rate of 300 $\mu$l/min using a syringe pump, and data acquisition was performed. A sensitivity of 160 ± 3 mV/pH was found for the sensor (Fig. 4(c)), which was much higher than the sensitivity of the electrochemical pH sensors based on IrOx thin films with a Nernstian and super-Nernstian response of 59 mV/pH and 62–77 mV/pH.[59,60]

In addition, the effect of flow rate on the sensitivity of the pH sensor was studied. DMEM with a pH value of 7.4 was perfused through the sensor using a syringe pump at various flow rates from 2 $\mu$l/min to 60 $\mu$l/min. As seen in Fig. 4(d), the sensor response was independent from the perfusion flow rate. Thus, the sensor can be adapted for microfluidic cell culture applications, in which a dynamic range of flow rates may be used for *in vitro* assessment of cellular functions.

### B. Characterization of the oxygen sensor

The sensor was characterized for measuring both gaseous and dissolved oxygen levels. As shown in Figs. 5(a) and 5(b) and S3 (see supplementary material),[51] the sensor had distinct

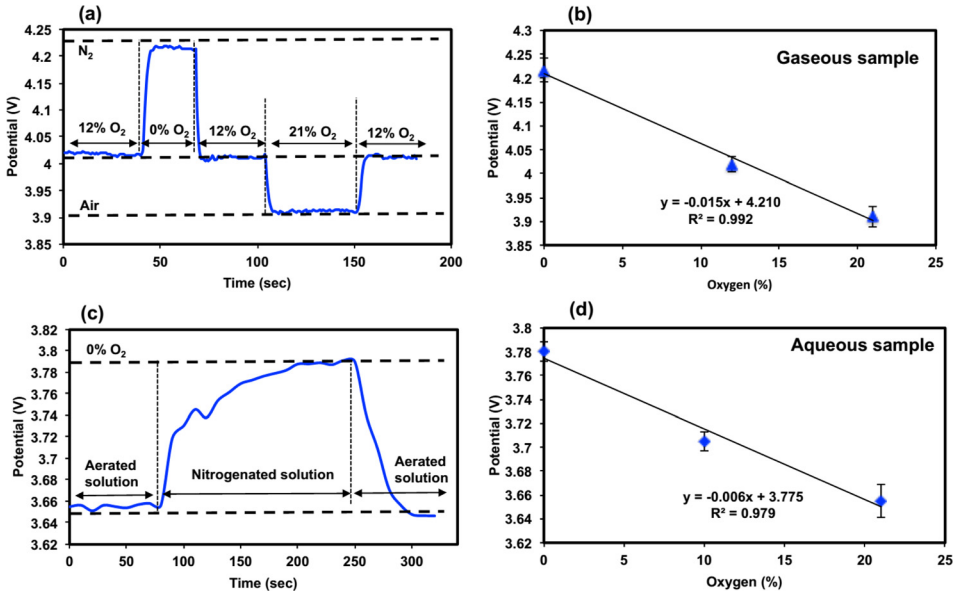


FIG. 5. Characterization of the oxygen sensor. (a) Response of the sensor to gaseous oxygen with different concentrations, (b) calibration curve for gaseous oxygen, (c) response of the sensor to dissolved oxygen in aerated and nitrogenated solutions, (d) calibration curve for dissolved oxygen.

reproducible responses to different gaseous oxygen concentrations. Also, the response of the sensor to different dissolved oxygen concentrations was characterized (Figs. 5(c) and 5(d)). To investigate the sensor characteristics, the detection channel was perfused using the aerated solution (21% $O_2$) for 80 s at a flow rate of 300 $\mu$l/min to quench the fluorophore. Once the sensor was perfused by a nitrogenated solution (0% $O_2$), the measured signal increased as a result of improvement in the level of fluorescent intensity. The signal amplitude decreased upon injection of an aerated solution to the sensor. The experiment was also carried out using a 1:1 mixture of aerated and nitrogenated solutions. A sensitivity of 6 mV/[%$O_2$] was determined using the current electronic setup for the measurement of dissolved oxygen concentrations. Comparison of Fig. 5(a) with Fig. 5(c) reveals that the dynamic sensor response was slower in aqueous solutions. The response time of the sensor in an aqueous environment could be limited by the rate of oxygen diffusion through the bulk liquid.[32] SNR value of the oxygen sensor was 36.3 dB. Using Arduino for data acquisition, the minimum detectable variation was 0.8 [%$O_2$], and the bandwidth was 0.03 Hz. SNR values for both pH and oxygen sensors indicate that they have a relatively noiseless nature for the measurements.

### C. Continual measurement of pH and oxygen in cell culture medium

#### *1. System validation*

The developed pH and oxygen sensors were fabricated on a single substrate with an optical window to measure pH value and dissolved oxygen level in a culture medium flowing through the bioreactor (Fig. 6(a)). Prior to performing the measurements, gas permeation through the bioreactor was characterized. Permeability of oxygen and $CO_2$ to the bioreactor is essential to provide sufficient oxygen for cellular functions and adjust pH in the flowing culture medium. The pH of DMEM is regulated using sodium bicarbonate in the presence of $CO_2$. As indicated in Eq. (1), the acidity (pH) of DMEM was adjusted using $CO_2$-bicarbonate based buffer[61]

$$CO_2 + H_2O \rightleftarrows HCO_3^- + H^+. \quad (1)$$

To evaluate gas permeation to the bioreactor, the system was operated using a stop-flow protocol, as explained in Section II G. Gas permeability experiments revealed that a continuous

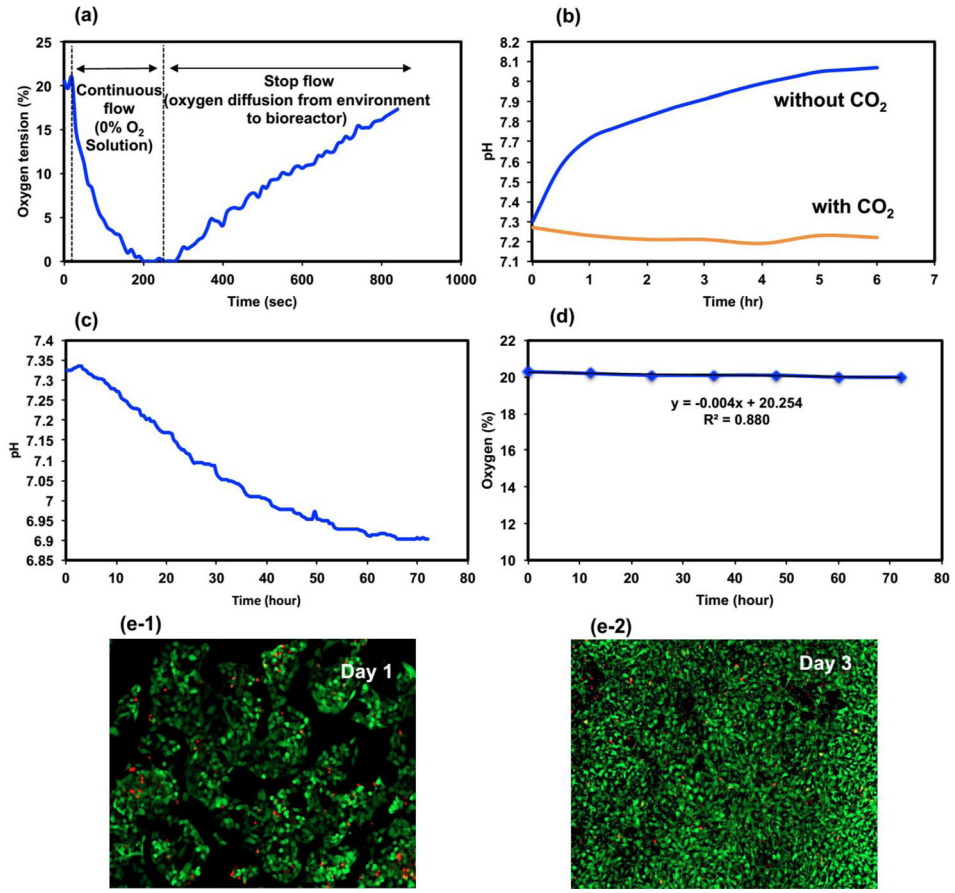


FIG. 6. Characterization of fabricated sensors, (a) characterization of oxygen permeability of the PDMS bioreactor using continuous flow and stop flow protocols, (b) pH measurements of the culture medium flowing through the bioreactor with no cells at the absence and presence of $CO_2$ supply, (c) continuous pH measurement of the culture medium flowing through the bioreactor with cultured HDFs cells, (d) continuous measurement of oxygen levels of the culture medium flowing through the bioreactor with cultured HDFs cells, (e-1) and (e-2) live-dead assay of cultured HDFs cells inside the bioreactor on day 1 and day 3, respectively.

decrease in oxygen concentration in the bioreactor was observed once it was perfused by a deoxygenated culture medium (Fig. 6(b)). The oxygen concentration eventually reached the minimum value, indicating zero dissolved oxygen tension in the bioreactor. Once the perfusion of the system with deoxygenated culture medium was stopped, a gradual increase in the oxygen tension inside the chamber was detected by the sensor due to diffusion of oxygen from the ambient air to the detection chamber. The oxygen tension increased to 21% as determined by the oxygen concentration of the ambient air. The rate of oxygen increase due to oxygen diffusion from the environment was lower than the rate of oxygen decrease by perfusing the chamber with nitrogenated solution (0% oxygen). This is mainly because of slower diffusion of ambient oxygen, which occurs through PDMS and the bulk solution in the detection chamber. Overall, it can be concluded that PDMS could provide continuous oxygenation of the culture medium, which is necessary for maintaining cellular activities.

Also, gas permeation of the bioreactor was further investigated using a continuous-flow protocol. To carry out the protocol, a microfluidic system was created which consisted of a peristaltic pump, a culture medium reservoir containing 1 ml DMEM, a pH sensor, and a bioreactor without cells (Fig. 1(e)). All of these components were interconnected using plastic tubing (Cole-Parmer, Teflon tubing, #30 AWG, inner diameter = 0.305 mm). The whole fluidic circuit was perfused at a flow rate of 20 $\mu$l/min. pH measurements were performed for 6 h at 37 °C in which the whole fluidic system was open to the ambient air. As shown in Fig. 6(b), the pH

value changed from neutral to alkaline over this period of time. The change of pH level to alkaline values was mainly associated with the lack of 5% $CO_2$ in the ambient air to buffer the culture medium. In comparison, when the experiment was conducted in the humidity incubator with 5% $CO_2$, the pH of the culture medium remained around neutral values. This occurred because $CO_2$ diffused into the bioreactor through the PDMS, mixed with the culture medium, and adjusted the pH of the culture media via the production of $CO_2$-bicarbonate buffer solution.

Taken together, these results clearly showed that the fluidic system was able to provide and maintain required oxygen and $CO_2$ into the culture medium. Moreover, the results demonstrated that the sensors could continuously measure the pH and dissolved oxygen levels in the cell culture medium.

### *2. Monitoring of pH and dissolved oxygen levels during cell culture*

The performance of the sensing module for continuous measurement of pH and dissolved oxygen levels was evaluated through its integration with a bioreactor containing cells. Initially, the bioreactor was seeded with HDFs ($4 \times 10^5$ cells), and it was kept in an incubator in static condition to produce an adherent layer of cells. Then, the bioreactor was integrated with the fluidic system for a continuous perfusion of culture medium at a flow rate of 200 $\mu$l/min. The change of acidification and oxygen level in the culture medium flowing through the bioreactor was monitored for 3 days, as shown in Figures 6(c) and 6(d). As shown in Fig. 6(c), the pH level of the culture medium continuously decreased during the perfusion experiment, which can be mainly associated with the cellular activities. As shown in Fig. 6(e), cells in the bioreactor maintained high viability. Over time, cellular metabolites including ammonia and lactate were accumulated inside the fluidic setup that shifted the pH towards acidic values.[47]

As for dissolved oxygen, the oxygen sensor showed a constant oxygen concentration within the solution during the course of the experiments, as shown in Figure 6(d). Although high cell viability and proliferation were observed over the microfluidic cell culture, no significant alteration in the concentration of the oxygen tension within the culture medium was observed. This could happen mainly due to continuous oxygen supply to the PDMS bioreactor, which is highly permeable to oxygen diffusion as discussed earlier. It is noteworthy to mention that the decrease in oxygen levels in the bioreactor could be due to insufficient oxygen supply to the bioreactor or oxygen buffering by the PDMS. Overall, the multi-analyte sensing module demonstrated a robust performance during 3 days of testing. This characteristic is beneficial for microfluidic cell culture applications.

## IV. CONCLUSIONS

This work describes the development of a multi-analyte microfluidic optical sensor employed to monitor pH and dissolved oxygen levels in cell culture medium perfused through a microfluidic bioreactor. Real-time pH monitoring of the bioreactor samples was achieved by detecting the level of light absorption by the phenol red available in the culture medium. Oxygen sensing was accomplished through measuring the degree of quenching in the luminescent intensity of an oxygen-sensitive flourophore. In addition, a low cost and user-friendly electronic interface was developed using an Arduino microcontroller platform. The sensors were tested investigating their linearity, optical stability, and accuracy. The compactness, ease of fabrication, and operation of the sensing module enabled its ideal adaption for microfluidic bioreactors and organ-on-chip applications. This optical system provides a non-invasive detection method with minimal maintenance after installation. Once integrated with a control system, the sensing module can indicate when circulating culture medium should be replaced with fresh medium (due to acidification, e.g., pH lower than 7) and how the oxygenation process (bioreactor in combination with an oxygenator) should be modulated once the oxygen level drops below a set point.

## ACKNOWLEDGMENTS

The authors gratefully acknowledge funding by the Defense Threat Reduction Agency (DTRA) under Space and Naval Warfare Systems Center Pacific (SSC PACIFIC) Contract No.

N66001-13-C-2027. The authors also acknowledge funding from the National Institutes of Health (EB012597, AR057837, DE021468, HL099073, and R56AI105024), and the Presidential Early Career Award for Scientists and Engineers (PECASE). Y.S.Z. acknowledges the National Cancer Institute of the National Institutes of Technology Pathway to Independence Award (1K99CA201603-01A1). The publication of this material does not constitute approval by the government of the findings or conclusions herein.

[1]S. N. Bhatia and D. E. Ingber, Nat. Biotechnol. **32**, 760 (2014).
[2]E. W. Esch, A. Bahinski, and D. Huh, Nat. Rev. Drug Discovery **14**, 248 (2015).
[3]D. Huh, Y. Torisawa, G. A. Hamilton, H. J. Kim, and D. E. Ingber, Lab Chip **12**, 2156 (2012).
[4]A. Polini, L. Prodanov, N. S. Bhise, V. Manoharan, M. R. Dokmeci, and A. Khademhosseini, Expert Opin. Drug Discovery **9**, 335 (2014).
[5]N. S. Bhise, J. Ribas, V. Manoharan, Y. S. Zhang, A. Polini, S. Massa, M. R. Dokmeci, and A. Khademhosseini, J. Controlled Release **190**, 82–93 (2014).
[6]Š. Selimović, M. R. Dokmeci, and A. Khademhosseini, Curr. Opin. Pharmacol. **13**, 829 (2013).
[7]Y. S. Zhang and A. Khademhosseini, Nanomedicine **10**, 685 (2015).
[8]N.-T. Nguyen, S. A. M. Shaegh, N. Kashaninejad, and D.-T. Phan, Adv. Drug Delivery Rev. **65**, 1403 (2013).
[9]I. Maschmeyer, A. K. Lorenz, K. Schimek, T. Hasenberg, A. P. Ramme, J. Hubner, M. Lindner, C. Drewell, S. Bauer, A. Thomas, N. S. Sambo, F. Sonntag, R. Lauster, and U. Marx, Lab Chip **15**, 2688 (2015).
[10]K. W. Barron, *Physiology (Oklahoma Notes)*, 4th ed. (Springer, New York, 1995).
[11]A. Lardner, J. Leukocyte Biol. **69**, 522 (2001).
[12]M.-H. Wu, J. P. G. Urban, Z. F. Cui, Z. Cui, and X. Xu, Biotechnol. Prog. **23**, 430 (2007).
[13]C. H. Orchard and J. C. Kentish, Am. J. Physiol. **258**, C967 (1990).
[14]R. K. Paradise, D. A. Lauffenburger, and K. J. van Vliet, PLoS One **6**, e15746 (2011).
[15]G. R. Martin and R. K. Jain, Cancer Res. **54**, 5670 (1994).
[16]G. Helmlinger, F. Yuan, M. Dellian, and R. K. Jain, Nat. Med. **3**, 177 (1997).
[17]M. D. Brennan, M. L. Rexius-Hall, L. J. Elgass, and D. T. Eddington, Lab Chip **14**, 4305 (2014).
[18]S. Lahiri, J. Appl. Physiol. **88**, 1467 (2000).
[19]M. Radisic, J. Malda, E. Epping, W. Geng, R. Langer, and G. Vunjak-Novakovic, Biotechnol. Bioeng. **93**, 332 (2006).
[20]M. Höckel and P. Vaupel, J. Natl. Cancer Inst. **93**, 266 (2001).
[21]V. I. Lushchak, T. V. Bagnyukova, V. V. Husak, L. I. Luzhna, O. V. Lushchak, and K. B. Storey, Int. J. Biochem. Cell Biol. **37**, 1670 (2005).
[22]B. Ungerböck, V. Charwat, P. Ertl, and T. Mayr, Lab Chip **13**, 1593 (2013).
[23]S. Sun, B. Ungerböck, and T. Mayr, Methods Appl. Fluoresc. **3**, 034002 (2015).
[24]Y. S. Zhang, J. Ribas, A. Nadhman, J. Aleman, S. Selimovic, S. C. Lesher-Perez, T. Wang, V. Manoharan, S.-R. Shin, A. Damilano, N. Annabi, M. R. Dokmeci, S. Takayama, and A. Khademhosseini, Lab Chip **15**, 3661 (2015).
[25]J. P. Wikswo, F. E. Block, D. E. Cliffel, C. R. Goodwin, C. C. Marasco, D. A. Markov, D. L. McLean, J. A. McLean, J. R. McKenzie, R. S. Reiserer, P. C. Samson, D. K. Schaffer, K. T. Seale, and S. D. Sherrod, IEEE Trans. Biomed. Eng. **60**, 682 (2013).
[26]C. Moraes, J. M. Labuz, B. M. Leung, M. Inoue, T.-H. Chun, and S. Takayama, Integr. Biol. **5**, 1149 (2013).
[27]R. Riahi, S. A. M. Shaegh, M. Ghaderi, Y. S. Zhang, S. R. Shin, J. Aleman, S. Massa, D. Kim, M. R. Dokmeci, and A. Khademhosseini, Sci. Rep. **6**, 24598 (2016).
[28]Y. S. Zhang, F. Busignani, J. Ribas, J. Aleman, T. N. Rodrigues, S. A. M. Shaegh, S. Massa, C. B. Rossi, I. Taurino, S.-R. Shin, G. Calzone, G. M. Amaratunga, D. L. Chambers, S. Jabari, Y. Niu, V. Manoharan, M. R. Dokmeci, S. Carrara, D. Demarchi, and A. Khademhosseini, Sci. Rep. **6**, 22237 (2016).
[29]G. M. Whitesides, Nature **442**, 368 (2006).
[30]N. P. Rodrigues, H. Kimura, Y. Sakai, and T. Fujii, in *Proceedings of the TRANSDUCERS EUROSENSORS'07—4th International Conference on Solid-State Sensors, Actuators Microsystems* (2007), Vol. 132, p. 843.
[31]A. Weltin, K. Slotwinski, J. Kieninger, I. Moser, G. Jobst, M. Wego, R. Ehret, and G. A. Urban, Lab Chip **14**, 138 (2014).
[32]A. P. Vollmer, R. F. Probstein, R. Gilbert, and T. Thorsen, Lab Chip **5**, 1059 (2005).
[33]D. B. Papkovsky and R. I. Dmitriev, Chem. Soc. Rev. **42**, 8700 (2013).
[34]E. A. Lima, R. M. Snider, R. S. Reiserer, J. R. McKenzie, D. W. Kimmel, S. E. Eklund, J. P. Wikswo, and D. E. Cliffel, Sens. Actuators, B **204**, 536 (2014).
[35]S. E. Eklund, R. M. Snider, J. Wikswo, F. Baudenbacher, A. Prokop, and D. E. Cliffel, J. Electroanal. Chem. **587**, 333 (2006).
[36]D. W. Kimmel, M. E. Meschievitz, L. A. Hiatt, and D. E. Cliffel, Electroanalysis **25**, 1706 (2013).
[37]D. W. Kimmel, W. P. Dole, and D. E. Cliffel, Biochem. Biophys. Res. Commun. **431**, 181 (2013).
[38]D. A. Markov, E. M. Lillie, S. P. Garbett, and L. J. McCawley, Biomed. Microdevices **16**, 91 (2014).
[39]S. A. M. Marzouk, S. Ufer, R. P. Buck, T. A. Johnson, L. A. Dunlap, and W. E. Cascio, Anal. Chem. **70**, 5054 (1998).
[40]I. A. Ges, B. L. Ivanov, D. K. Schaffer, E. A. Lima, A. A. Werdich, and F. J. Baudenbacher, Biosens. Bioelectron. **21**, 248 (2005).
[41]C.-C. Wu, W.-C. Lin, and S.-Y. Fu, Biosens. Bioelectron. **26**, 4191 (2011).
[42]Y. Cheng, P. Xiong, C. S. Yun, G. F. Strouse, J. P. Zheng, R. S. Yang, and Z. L. Wang, Nano Lett. **8**, 4179 (2008).
[43]W. Zhan, G. H. Seong, and R. M. Crooks, Anal. Chem. **74**, 4647 (2002).
[44]A. Richter, G. Paschew, S. Klatt, J. Lienig, K.-F. Arndt, and H.-J. P. Adler, Sensors **8**, 561 (2008).
[45]D. Wencel, T. Abel, and C. McDonagh, Anal. Chem. **86**, 15 (2014).
[46]Z. Liu, J. Liu, and T. Chen, Sens. Actuators, B **107**, 311 (2005).
[47]S. Lee, B. L. Ibey, G. L. Coté, and M. V. Pishko, Sens. Actuators, B **128**, 388 (2008).

[48]E. B. Magnusson, S. Halldorsson, R. M. T. Fleming, and K. Leosson, Biomed. Opt. Express **4**, 1749 (2013).
[49]X. Wang and O. S. Wolfbeis, Chem. Soc. Rev. **43**, 3666 (2014).
[50]P. Lehner, C. Staudinger, S. M. Borisov, and I. Klimant, Nat. Commun. **5**, 4460 (2014).
[51]See supplementary material at http://dx.doi.org/10.1063/1.4955155 for the fabrication and characterization of the Sensing.
[52]I. J. Koenka, J. Sáiz, and P. C. Hauser, Chim. Int. J. Chem. **69**, 172 (2015).
[53]P. L. Urban, Analyst **140**, 963 (2015).
[54]E. T. da Costa, M. F. Mora, P. A. Willis, C. L. do Lago, H. Jiao, and C. D. Garcia, Electrophoresis **35**, 2370 (2014).
[55]R. Fobel, C. Fobel, and A. R. Wheeler, Appl. Phys. Lett. **102**, 193513 (2013).
[56]G. Mehta, K. Mehta, D. Sud, J. Song, T. Bersano-Begey, N. Futai, Y. S. Heo, M.-A. Mycek, J. Linderman, and S. Takayama, Biomed. Microdevices **9**, 123 (2007).
[57]J. de Jong, R. G. H. Lammertink, and M. Wessling, Lab Chip **6**, 1125 (2006).
[58]M. Jansen, *Noise Reduction by Wavelet Thresholding* (Springer, New York, 2001).
[59]P. Kurzweil, Sensors (Switzerland) **9**, 4955 (2009).
[60]S. Głab, A. Hulanicki, G. Edwall, and F. Ingman, Crit. Rev. Anal. Chem. **21**, 29 (1989).
[61]P. Eibl, R. Eibl, D. Pörtner, R. Catapano, and G. Czermak, *Cell and Tissue Reaction Engineering* (Springer-Verlag, Berlin, Heidelberg, 2009).